Available online at www.sciencedirect.com

ScienceDirect

journal homepage: www.ejcancer.com

ELSEVIER

Original Research

Tumour infiltrating B cells discriminate checkpoint blockade-induced responses

Sara Valpione [a,b,**], Luca G. Campana [c], John Weightman [d], Zena Salih [a,b], Elena Galvani [a], Piyushkumar A. Mundra [a], Francesco De Rosa [e], Avinash Gupta [b], Patricio Serra-Bellver [b], Paul Lorigan [b], Theodora Germetaki [b], Marek Dynowski [f], Stephen Kitcatt [f], Sudhakar Sahoo [g], Dave Lee [g], Nathalie Dhomen [a], Graham Lord [h], Richard Marais [a,*]

[a] *Molecular Oncology Group, Cancer Research UK Manchester Institute, The University of Manchester, Alderley Park SK10 4TG, United Kingdom*
[b] *The Christie NHS Foundation Trust, 550 Wilmslow Road, Manchester M20 4BX, United Kingdom*
[c] *Department of Surgery, Manchester University NHS Foundation Trust, Manchester, United Kingdom*
[d] *Molecular Biology Core Facility, Cancer Research UK Manchester Institute, The University of Manchester, Alderley Park SK10 4TG, United Kingdom*
[e] *Immunotherapy and Rare Tumours Unit, Istituto Scientifico Romagnolo per Lo Studio e La Cura Dei Tumori (IRST) "Dino Amadori" IRCCS, Meldola (FC) 47014, Italy*
[f] *Scientific Computing, Cancer Research UK Manchester Institute, The University of Manchester, Alderley Park SK10 4TG, United Kingdom*
[g] *Computational Biology Support Team, Cancer Research UK Manchester Institute, The University of Manchester, Alderley Park SK10 4TG, United Kingdom*
[h] *School of Biological Sciences, Faculty of Biology, Medicine and Health, The University of Manchester, United Kingdom*

Abstract *Background:* Immune cell-driven anti-cancer activity is paramount for effective responses to checkpoint inhibitors (ICB). However, the contribution of the different immune cell subsets in the circulation and within the tumour is poorly understood.
Materials and methods: To elucidate the role of the different cell subsets in anti-tumour responses elicited by ICB, we performed single-cell analysis of the transcriptome and surface

* *Corresponding author*. Molecular Oncology Group, Cancer Research UK Manchester Institute, The University of Manchester, Alderley Park SK10 4TG, United Kingdom.
** *Corresponding author*. Molecular Oncology Group CRUK Manchester Institute
The University of Manchester Alderley Park SK10 4TG, United Kingdom.
E-mail address: sara.valpione@cruk.manchester.ac.uk (S. Valpione), richard.marais@cruk.manchester.ac.uk (R. Marais).

proteome of paired pre- and early on-treatment metastatic melanoma tumour biopsies and matched peripheral blood mononuclear cell samples. We next compared the survival of metastatic melanoma patients treated with ICB according to the abundance of pre-treatment tumour-infiltrating B cell clonotypes.

Results: We identified cell clusters associated with disease control or progression, defined differential expression of biological pathways likely involved in the immune awakening against the tumour and examined how cell—cell communication patterns between the tumour cell subsets change during treatment. Furthermore, we discovered that B cells (immunoglobulin expression and abundance of B cell clonotypes) discriminate the clinical response after ICB and propose that B cells likely contribute to anti-tumour immunity by antigen presentation through major histocompatibility complex molecules. Finally, we demonstrated that the abundance of tumour-infiltrating B cell clonotypes at baseline identifies two distinct risk groups, a finding that we confirmed in an independent cohort.

Conclusions: Our exploratory translational study provides new insights on the mechanistic role of B cells in anti-melanoma immunity during treatment with ICB. Additionally, we support pre-treatment B cell tumour infiltration as a promising prognostic biomarker to be further validated as a tool for clinical risk stratification.

1. Introduction

Immune checkpoint blockade (ICB) has become a new standard of care in cancer [1], making the identification of reliable prognostic and predictive biomarkers and mechanistic studies of response and refractoriness current research priorities in oncology. Cellular immunity is paramount to effective response to ICB [2], but the stimulatory or suppressive role of different cell subsets in the circulation and tumour infiltrate is still poorly understood. We previously demonstrated that pre-treatment T cell receptor (TCR) clonality of tumour infiltrating T cells (TIL/Tc) discriminates risk groups and predicts response and survival in patients with advanced melanoma receiving ICB [3]. We also showed that treatment-induced reduction of T cell clonal relatedness of the clonotypes shared between the tumour and periphery predicts response with ICB. These findings suggest that the tumour-infiltrating and peripheral immune cell pools are distinct, although not isolated, compartments and must be studied to understand ICB effects.

Here, we investigated the milieu of the circulating and tumour infiltrating immune cells, their function and possible mechanisms of therapeutic response and refractoriness. We performed single-cell RNA expression and protein sequencing (REAP-Seq) of longitudinal tumour and peripheral blood mononuclear cell (PBMC) samples taken before and after one cycle of ICB. We identified distinct CD-14 monocyte clusters associated with treatment response, and we showed that B cells discriminated patients who responded to treatment from those who did not. By expanding our analysis to two independent cohorts of pre-treatment melanoma samples, we showed that the abundance of B cell clonotypes was prognostic for overall survival.

2. Materials and methods

Study design and patient cohort: This was a longitudinal non-interventional biomarker study. The patients received first line standard of care anti-PD1 based immunotherapy at the Christie NHS Foundation Trust (NCT04493723, BioBank ethics application #18/NW/0092; MCRC Biobank Access Committee application 13_RIMA_01). All patients gave written informed consent to the study and all clinical investigations were conducted according to the principles expressed in the Declaration of Helsinki and good clinical practice guidelines. Patient inclusion criteria were treatment naïve patients with metastatic or inoperable locally advanced melanoma undergoing first-line therapy with standard of care. Exclusion criteria were previous malignancy, autoimmune disease, systemic infectious disease at the time of sample collection and treatment with immunosuppressant drugs.

Sample size calculation for single-cell analyses and survival analysis: power calculation performed with SCOPIT (v.1.1.4) [4] estimated a probability >95% to detect cell populations of interest with as few as 10 cells per sample; scPower [5] calculated a detection power for differential expression of 0.71 in our dataset. Sample size for survival analysis was not pre-set; all available melanoma metastasis samples in our BioBank from treatment naïve patients treated with first line anti-PD1 drugs and not taking immunosuppressants were analysed (N = 20, alpha = 0.05, beta = 0.6), and in the validation cohort [6] (N = 120, alpha = 0.05, beta = 0.8). Investigators were blinded during experiments and outcome assessment performed after experiments. Response to treatment was assessed at 12 weeks after the first cycle infusion by radiographic imaging using RECIST 1.1; disease control was defined as complete response, partial response, or

stable disease. Cells that did not pass the quality check with standard single-cell RNA-Seq mitochondrial and mRNA feature filtering were excluded; a maximum upper boundary of 18% mitochondrial genes was set based on the standard deviation within the cohort. Biopsies from patient #RM160 were not included because no cells from the baseline sample passed the quality check and the patient declined to undergo the W3 biopsy. No outliers were excluded from the downstream analyses.

Single cell preparation and sequencing: Peripheral blood was collected in 10 mL EDTA blood tubes on ice during transport from the hospital to the laboratory (target transport time <1 h). PBMC were immediately separated using Sep Mate and Lymphoprep following manufacturer's instructions (StemCell Technology, cat 85, 450 and 07801). Melanoma metastases biopsies were performed according to the hospital good clinical practice standard operating procedures and immediately transported (target transport time <1 h) to the laboratory in ice cold MACS Tissue Storage Solution (Miltenyi Biotechnologies, cat 130-100-008) for single cell suspension preparation using MACS Tumour Dissociation kits for human samples according to manufacturer's manual (Miltenyi Biotechnologies, cat 130-095-929). PBMCs and the tumour single-cell suspension were processed for labelling with BioLegend TotalSeq antibodies (Supp. Table 1) according to manufacturer instructions 'protocol A' (Chromium 10X 3′ kits). Labelled single-cell suspensions were loaded onto Chromium Chip B (10x Genomics, PN-1000073) and a gel bead emulsion was generated on the 10x Chromium Controller using the Chromium Single Cell 3′ GEM, Library & Gel Bead Kit v3 (10x Genomics, PN-1000075) according to the manufacturer's protocol. Gene expression and TotalSeq-A ADT libraries were produced according to the Bio-Legend Totalseq-A protocol and 10x Genomics user guide. Library quality was checked using the Agilent Bioanalyzer and quantified by qPCR using a KAPA Library Quantification Kit for Illumina sequencing platforms (Roche, cat no. 07960336001). Paired-end sequencing was performed by clustering the pooled library on an Illumina NextSeq 500 system in High Output mode with read lengths of 28 + 8+101 cycles.

Generating count matrices from fastQ. Transcriptomic count matrices were generated from fastQ files through the 10x genomics *cellranger* pipeline [7] using the *count* method. If the same 10x libraries was used in multiple sequencing runs they were combined with *cellranger*'s *count* method through specifying the location of each separate run as input. For cases where different 10x libraries were requested to be combined; *cellranger*'s '"*aggr*" function was used. *Cellranger* version 3.1.0 was used and data searched against human transcriptome as a reference (refdata-cellranger-GRCh38−3.0.0).

Generating ADT count matrices from fastQ ADT count matrices were generated through processing of ADT-derived fastQ files with Cite-Seq-Count (v.1.4.2) software [8,9]. This software required read structure details (locations of UMI and barcodes within reads), a tag list containing sequences corresponding to unique antibodies (ADTs; Supp. Table 1) and estimated cell numbers and cellular barcodes (determined through *cellranger-count* processing of the scRNA counterpart). FastQ files for individual samples were concatenated across lanes respectively and used as input along with the above requirements to generate ADT-derived counts corresponding to scRNA data and therefore enable integration of RNA and protein for downstream analysis [7,8].

RNA-Seq Bulk RNA-Seq data were processed as described elsewhere [3]. BCR sequences were reconstructed from bulk RNA-Seq using ImRep as described elsewhere [3]. Single cell analyses were performed on sequential peripheral blood and tumour biopsy samples as per BioLegend and Chromium 10X standard operating procedures for 3' CITE-Seq with TotalSeq-A antibodies.

Statistics and bioinformatics: Statistics analyses and graphics generation were performed with GraphPad Prism version 9 (GraphPad Software, La Jolla California USA), R Studio Workbench (v. 1.4.1717−3, The R Foundation for Statistical Computing, Vienna, Austria) and R packages for R v.4.1 (*tidyverse, rms, survminer, Seurat v.4, Harmonize, EnhancedVolcano, enrichR, viridis, cowplot* and dependencies) and CellPhoneDB python package [10]. DE was performed with MAST, and p-values adjusted with Bonferroni correction. GO biological pathway visualisation for Supp. Fig. 3 and 4 was performed using *g:Profiler* [11,12].

3. Results

3.1. Patient samples

We performed REAP-Seq on 58,426 good quality single cells obtained from pre-treatment (T0) and paired on-treatment (week 3/W3, after the first cycle of treatment) matched PBMC and tumour biopsy samples from 5 treatment-naïve metastatic melanoma patients (patient characteristics and response to treatment are reported in Supp. Table 2). After exclusion of poor-quality cells, the data was processed with *SCTransform* [13] and corrected for batch effects with *Harmony* [14] (Supp. Fig. 1A-D).

3.2. Identification of PBMC signatures associated with ICB responses

First, we analysed the PBMC data. UMAPs (uniform manifold approximation projection) revealed two distinct PBMC clusters (clusters 1 and 2) that were present at T0 but not W3 (Fig. 1A). Notably, cluster 1 was present only in patients who developed progressive disease (PD), whereas cluster 2 was present only in patients who achieved disease control (DC) (Fig. 1B). Using an annotated reference dataset of 211,000 cells [15] (Supp. Fig. 1E) we identified the cells in both clusters 1 and 2 as subsets of CD14$^+$
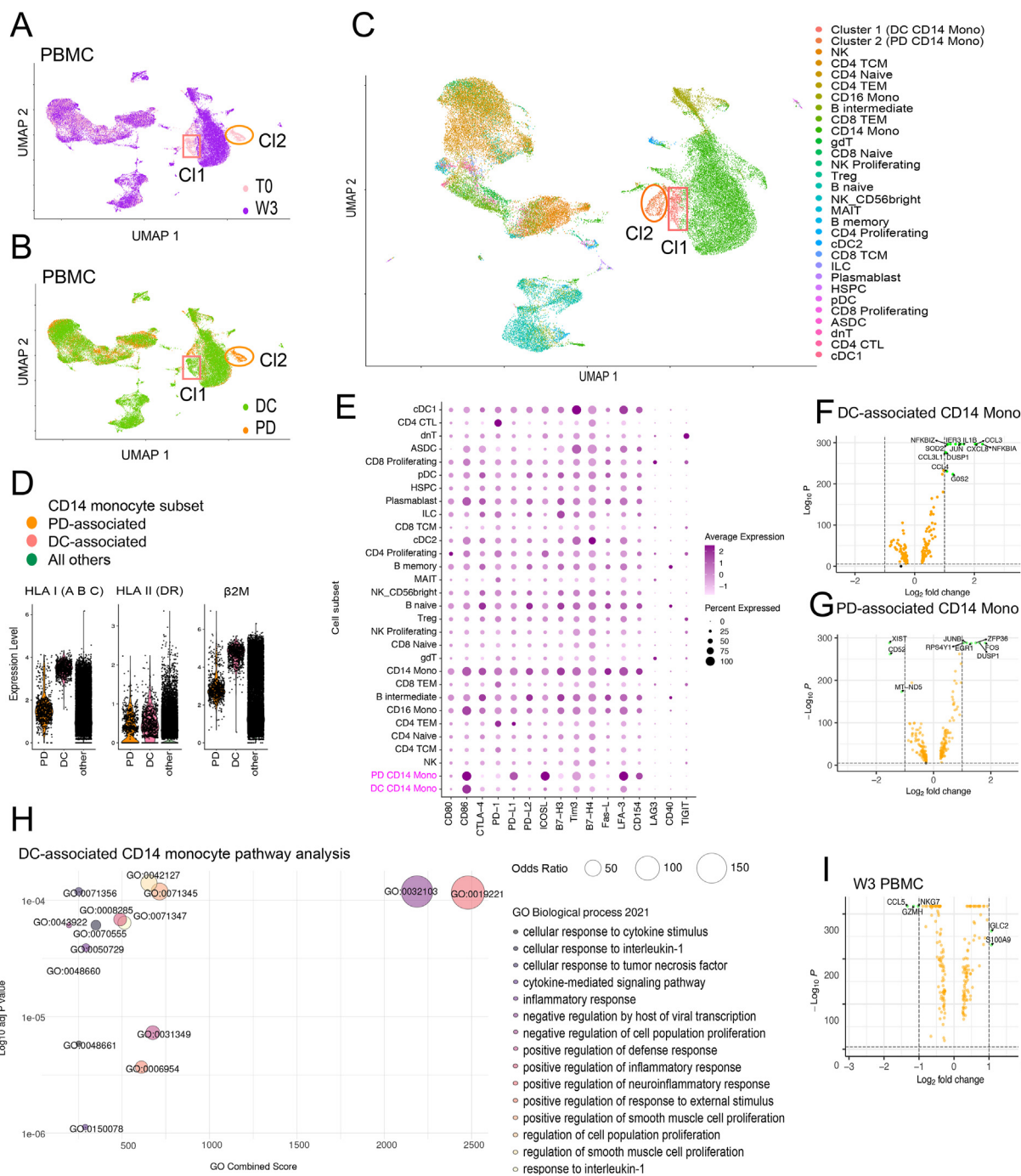
Fig. 1. Identification of PBMC signatures associated with ICB responses (A–C) UMAPs of single cell RNA-Seq of 48,684 PBMCs coloured according to timepoint (A), W12 response (B), and cell cluster identity (C; *predictcellidentity.l2*). Cluster 1 and cluster 2 are highlighted in (A), (B) and (C) by the orange square and pink circle respectively. Cell identities in (C) are indicated by the colour coded legend (D) Violin plot showing HLA (A,B,C) surface protein expression levels in DC-associated, PD-associated and other CD14 monocytes (E) Dot plot showing average expression (colour scale = expression intensity) of surface protein or mRNA (*LAG3*, *CD40* and *TIGIT*) and percentage of positive cells (dimension scale = proportion of positive cells) for selected surface checkpoint inhibitor and stimulatory molecules (F) Volcano plot showing differentially expressed genes in DC-associated versus other CD14 monocytes at T0. (G) Volcano plot showing differentially expressed genes in PD-associated versus other CD14 monocytes at T0 (H) Scatter plot showing GO combined score and Log_{10} adjusted p-value for the top 15 biological processes upregulated in DC-associated versus PD-associated CD14-monocytes (dot size = Odds Ratio, OR) (I) Volcano plot showing differential expression in PBMCs at W3 in patients who achieved DC versus PD. T0 = pre-treatment; W3 = week 3; PD = progressive disease; DC = disease control; HLA = human leucocyte antigen; GO = gene ontology. (F), (G), (I): orange dots = genes with adjusted p-value < 0.05 but fold change $Log_2<1$, green dots = genes with adjusted p-value < 0.05 and fold change $Log_2<1$).

monocytes (CD14-monocytes) (Fig. 1C). Note that compared to other circulating CD14−monocytes, the PD and DC-associated CD14-monocyte populations both expressed higher levels of human leukocyte antigen (HLA) class I and II on their surface, although HLA class I and II expression was higher on DC-associated than PD-associated CD14-monocytes (Fig. 1D). Moreover, expression levels and the positive cell proportion for the surface regulatory checkpoint molecules PD-L1, ICOSL, LF3 and CD154 (CD40-L) were higher in PD-associated than DC-associated CD14-monocytes (Fig. 1E).

Compared to bulk CD14-monocytes, the DC-associated CD14-monocytes displayed significant upregulation of genes involved in acute phase inflammatory cytokine production (*IL8*, *IL1B*), chemotaxis (*CCL3L1*, *CCL4*, *CCL3*) and NF-kB regulation (*NF-kBIA*, *NF-kBIZ*, *IER3*) (Fig. 1F), whereas the PD-associated CD14-monocytes showed upregulation of differentiation stage markers (*JUNB*, *FOS*, *EGR1*) and the inflammation inhibitor ZFP36 (tristetraprolin [16]), but downregulation of the adhesion factor CD52 (CAMPATH) (Fig. 1G). These observations were consistent with pathway analysis showing that, compared to PD-associated CD14-monocytes, DC-associated CD14-monocytes upregulated biological processes involved in the effector inflammatory acute phase (Fig. 1H). Note that single-cell sequencing at W3 did not reveal changes in monocytic gene expression in DC versus PD patients, although, curiously, in the DC patients, there was reduced expression of genes involved in acute cytotoxicity (*CCL5*, *NGK7*, *GZMH*) and upregulation of the inflammatory gene *SL100A9* and the B cell gene *IGLC2* (Fig. 1I).

3.3. Tumour and immune-microenvironment signatures associated with ICB responses

Next, we analysed the tumour biopsy data. We used RNA and surface protein expression of lymphocytes (CD3, CD8a, CD4, NKG2D, *NKG7*, *MS4A1*, CD20, CD19, *FCGR3A*) and monocyte/macrophage (CD14, *GNLY*, *MS4A7*, *FCER1A*, *LYZ*, CD11b, CD16) markers to separate the tumour infiltrating immune mononuclear cells (TIMC) from the other tumour cells (melanoma and other stroma cells). Note that subsequent transcriptome analysis of the melanoma and stroma cells at W3 revealed that the DC tumours were characterised by, amongst other genes, downregulation of apolipoproteins, melanocyte and serpin genes, and upregulation of insulin growth factor binding protein 2, retinoic acid pathway (*RBP1*, *CRABP2*), pro-inflammatory genes (*IL32*, *CCL5*) and cytoskeleton contractility genes (Suppl. Fig. 2A and B).

More pertinent, to study the determinants of effective immune-awakening in the immune-infiltrate we focussed on the TIMC. Unlike the PBMC UMAPs, the TIMC UMAPs at T0 versus W3 (Fig. 2A) in patients who developed PD versus DC (Fig. 2B) did not identify any response-associated clusters. However, transcriptome analysis at W3

revealed significant differences between PD- and DC-patient TIMCs. Specifically, the latter had downregulation of, among others, genes that drive early T cell stimulation (e.g. *JUN*, *FOS*, *CD69*), chemotaxis (e.g. *CCL4*) and monocyte/macrophage inflammation (*DUSP1* and *DUSP2*) together with upregulation of complement *C1QA*, and the B cell genes *MZB1* (which enables efficient antibody secretion) and Ig genes, with both IgM and post-isotype switch IgA and IgG heavy chains (Fig. 2C).

3.4. B cell signatures associated with ICB-induced responses

Intrigued by this finding, we investigated the role of B cells in ICB-induced immune-responses. First, we assigned an identity to each TIMC using the annotated reference and then compared them for expression of a panel of surface proteins involved in co-stimulatory and checkpoint inhibitor activity. In general, compared to the other TIMC, the B cell compartment had lower levels of surface co-stimulatory and checkpoint inhibitor regulatory molecules (Fig. 2D). In particular, the B cells had the lowest surface expression of PD-1 and PD-L2 and the second lowest surface expression of PD-L1, making it unlikely that they are direct targets of anti-PD-1 drugs or that they mediate T cell suppression driven by the PD-L1/PD-L2 interaction with PD-1 in the tumour microenvironment.

In addition to producing Ig, B cells present antigens to T lymphocytes [17], so we investigated if different tumour infiltrating B cells expressed human leukocyte antigen (HLA) molecules. Intriguingly, compared to all other TIMCs, the memory B cells had the highest surface expression of both class I (A, B, C and β2microglobulin) and class II (DR) HLA (Fig. 2E), making these cells potential candidates for effective neoantigen cross-presentation. The importance of antigen presentation by this population was supported by GO pathway analysis which revealed that '*antigen processing'*'and '*expression of peptide antigens on class I HLA*' (both TAP1 dependent and independent) were the most differentially activated biological processes in DC-associated compared to PD-associated memory B cells (Fig. 2F).

To dissect the role of B cells in ICB-induced anti-cancer responses, we investigated the interaction networks between B cells, other TIMC, melanoma and stroma cells in the biopsies. For this, we used marker genes to identify melanoma cells (*MITF*+, *TYR*+), endothelium (CD31+), activated fibroblasts (*FAP*+) and other tumour stroma cells (negative for *MITF*, *TYR*, *CD31*, or *FAP*, lymphocyte and monocyte/macrophage markers) and then used CellPhoneDB to estimate ligand/receptor communications between all biopsy cells. At T0, the most connected cells were the *FAP* + fibroblasts and CD31+ cells, which had predicted ligand/receptor interactions with most other cell clusters (Fig. 3A). Amongst the B cells, the memory B cells had the most abundant and intense predicted interactions with other cells, particularly the *FAP*+ fibroblasts, CD31+ cells, CD8

Fig. 2. Identification of tumour immune-infiltrate signatures associated with ICB responses (A, B) UMAPs of single cell RNA-Seq of 9910 TIMC coloured according to timepoint (A) or patient response at week 12 (B) (C) Volcano plot showing differential expression of TIMCs in patients who achieved DC versus PD (orange dots = genes with adjusted p-value < 0.05 but fold change $Log_2 < 1$, green dots = genes with adjusted p-value < 0.05 and fold change $Log_2 < 1$) (D) Violin plots showing surface protein expression levels or mRNA (*LAG3*, *CD40*, *TIGIT*) for selected surface checkpoint inhibitor and stimulatory molecules in TIMC cell clusters (*predictcellidentity.l1*) (E) Violin plots showing the expression level of HLA surface proteins in the TIMC cell clusters (*predictcellidentity.l2*) at both timepoints. (F) Scatter plot showing GO combined score and Log_{10} adjusted p-value for the top 15 biological processes upregulated in memory B cells in TIMC of patients who achieved DC versus PD; dot size represents OR.TIMC = tumour infiltrating mononuclear cells; T0 = pre-treatment; W3 = week 3; PD = progressive disease; DC = disease control; HLA = human leucocyte antigen; GO = gene ontology.

Fig. 3. Cell communication network in the tumour biopsies estimated by CellPhoneDB (A, B) Heatmap of predicted communication networks between tumour biopsy cell clusters at T0 (A) and W3 (B). Colour scale indicates the number of predicted interactions (C, D) List of interacting molecules for communications of B cell clusters at T0 (C) and W3 (D); dimension scale is inversely proportional to Log_{10} p-values and colour scale indicates the means of the average expression level of interacting molecule 1 in 'cell 1' and interacting molecule 2 in 'cell 2' on the X-axis.
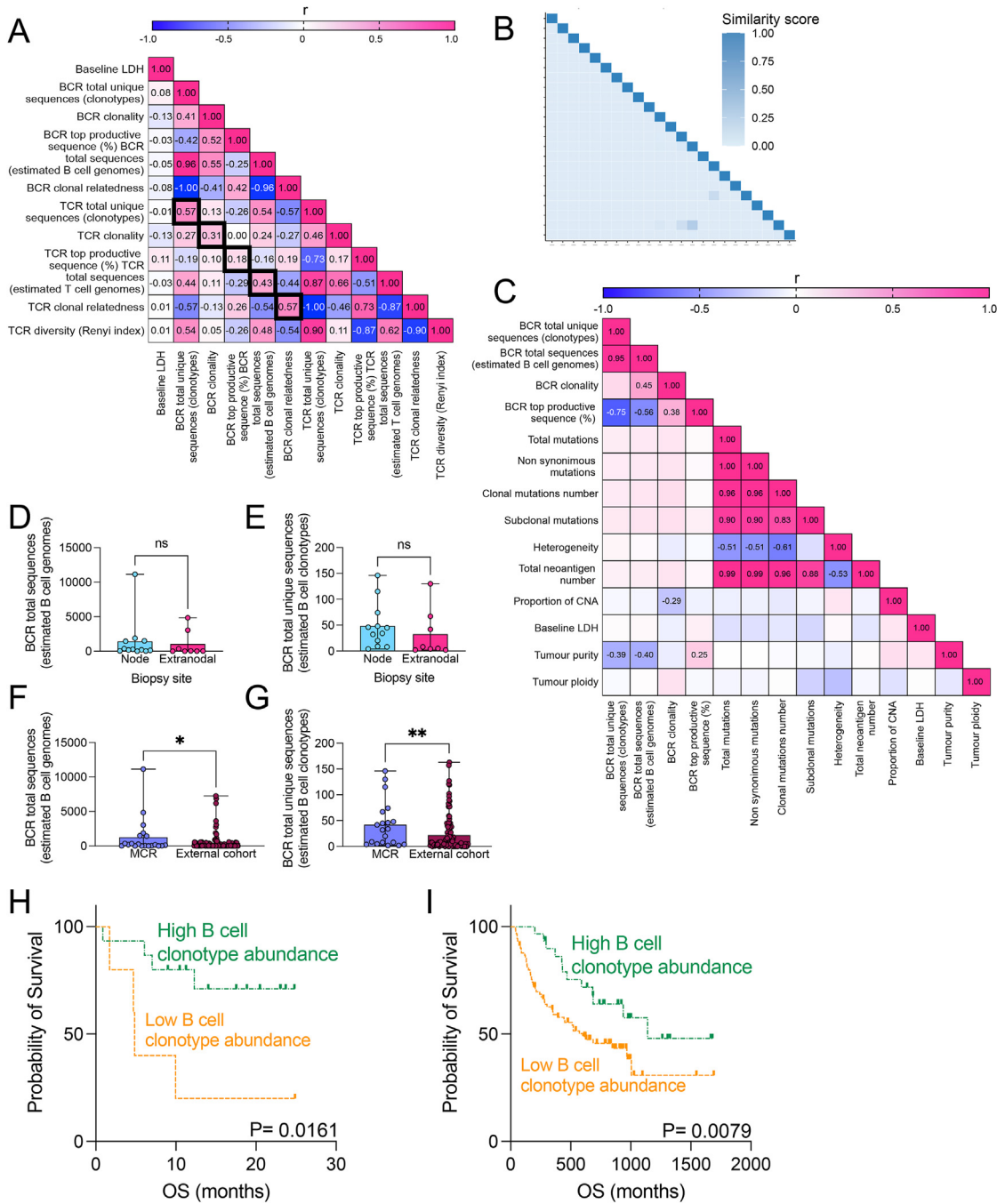
Fig. 4. Prognostic value of tumour infiltrating B cell clonotype abundance (A) Heatmap showing correlation between LDH, TCR and BCR metrics (sequences reconstructed from bulk RNA-Seq) in our 20 pre-ICB melanoma biopsy cohort (colour scale = Spearman r square, also reported in the heatmap) (B) Similarity matrix for BCR sequences of samples from (A) (colour scale = Bhattacharya index) (C) Heatmap showing the correlation between LDH, BCR metrics (sequences reconstructed from bulk RNA-Seq) and mutations in the validation cohort of 120 pre-ICB melanoma samples (colour scale = Spearman r square, also reported in the heatmap for correlations with p-value < 0.05) (D, E) Graphs showing the number of BCR total sequences (D) (Mann−Whitney test P = 0.279; median = 234 and 36) and number of BRC unique sequences (E) (clonotypes; Mann−Whitney test P = 0.151; median = 40 and 7) from the series shown in (A) according to the biopsy site (blue = nodal, pink = extra-nodal) (F, G) Graphs showing number of BCR total sequences (F) (Mann−Whitney test P = 0.032; median = 189 and 42) and the number of BRC unique sequences (G) (clonotypes) from the series analysed in (A, lilac) and (C, maroon) (Mann−Whitney test P = 0.008; median = 33 and 6) (H, I) Survival curves of patients treated with ICB drugs with high (green) or low (orange) pre-treatment TIL/Bc clonotype abundance in our training cohort (A) (H; log-rank P = 0.017, median survival not reached versus 4.8 months) and the external validation cohort (C) (I; log-rank P = 0.025, median survival = 1139 versus 600 months). D, E, F, G: center line, median; box limits, upper and lower quartiles; whiskers, range. LDH = lactic dehydrogenase; TCR = T cell receptor; BCR = B cell receptor; ns = not significant.

naïve T cells, Tregs, CD14$^+$ and CD16$^+$ monocytes/macrophages, other less mature B cell subsets, and the HSPC and ASDC niche (Fig. 3A). At W3, the memory B cells no longer interacted with FAP^+ fibroblasts or CD31$^+$ cells but had predicted ligand/receptor interactions with most other cell subsets, with the notable exception of other B cells, and NK and central memory CD8$^+$ T cells (Fig. 3B). At T0, interactions were predominantly driven by cell adhesion, homing molecules and extracellular matrix/epithelial-to-mesenchymal transition regulation (Fig. 3C and Supp. Fig. 3), whereas at W3, the interaction network still contained adhesion and homing molecules, but also TNF family signalling, HLA class II (HLA-DPB1) and co-stimulus/suppressive regulation (Fig. 3D and Supp. Fig. 4).

3.5. Prognostic value of B cell clonotype abundance

Finally, to investigate if tumour infiltrating B cells (TIL/Bc) were prognostic for response to ICB, we applied the approach we previously used to analyse tumour infiltrating T cell (TIL/Tc) subclones to the B cell compartment [3,18].

We used ImRep [19] to analyse bulk RNA-Seq data and reconstructed the complementarity determining region 3 of B cell receptor (BCR) and T cell receptor (TCR) sequences in a series of 20 pre-treatment micro-dissected melanoma metastasis samples from Manchester, Padova and Meldola. We compared the TIL/Bc and TIL/Tc repertoires and observed an overall concordance between the BCR and TCR metrics (r = 0.57 for total number of clonotypes, 0.31 for clonality, 0.18 for % representation of the top productive sequence, 0.43 for total number of genomes, 0.57 for clonal relatedness, Fig. 4A, black highlights). The Bhattacharya similarity score of the BCR sequences was negligible for all pairwise comparisons (Fig. 4B), suggesting that the TIL/Bc infiltrates were predominantly private.

To study correlations between BCR repertoire metrics and mutational landscape, we used ImRep to reconstruct BCR sequences from bulk RNA-Seq in pre-treatment biopsies from a published cohort of 120 metastatic melanoma patients treated with ICB and for which DNA sequencing data was available [6]. We observed an intuitive inverse correlation between tumour purity and BCR abundance (r = −0.39 for total clonotypes, −0.40 for total sequences) and a direct correlation between tumour purity and top BCR clone prevalence (r = 0.25), suggesting high convergence when few clones were present (Fig. 4C). There was also an inverse correlation between BCR clonality and copy number alteration (r = −29), but no significant correlation between BCR repertoire metrics and the number of total, non-synonymous, clonal or subclonal mutations, mutation heterogeneity and neoantigen number (Fig. 4C). To exclude possible confounding factors from tissues physiologically rich in lymphocytes, we compared the total number of BCR sequences (Fig. 4D) and clonotypes (Fig. 4E) in the nodal and extra-nodal metastases in our cohort and found no significant differences, suggesting that tumour infiltration by TIL/Bc was not influenced by lymph-node microenvironments. Finally, we tested if the abundance of distinct BCR clonotypes, possibly recognising different neoantigens, correlated with survival and found that, despite differences in the number of BCR clonotypes (number of unique sequences) (Fig. 4F) and total sequences (Fig. 4G), the abundance of BCR clonotypes was a favourable prognostic factor in both our 20-patient training cohort (Fig. 4H) and the published 120-patient validation cohort (Fig. 4I).

4. Discussion

ICB has revolutionised melanoma care over the last decade. It is approved in advanced disease, for adjuvant care in stage III and is currently being trialled in the stage II adjuvant setting (NCT03553836 [20], NCT04309409). However, in both the advanced and adjuvant setting there is an urgent need for predictive and prognostic stratification tools to refine patient care, particularly in intermediate-risk patients for whom the odds of toxicity could outweigh the benefit of treatment. We previously defined T cell and TCR repertoire evolution under ICB as prognostic and predictive in this disease, and here we extend those studies to reveal that CD-14 monocyte subsets and B cell signatures are also prognostic for melanoma patients.

First, we identify two clusters of peripheral CD14-monocytes in melanoma patients at baseline. Cluster 1 was present only in patients who then experienced disease progression, whereas cluster 2 was only in patients who responded. Note that both clusters were absent at W3 of treatment, suggesting that both reacted to ICB. Moreover, cluster 2 displayed evidence of upregulated effector inflammatory acute phase genes and hyper-activated IL1 signalling, an observation that is consistent with acute inflammation pre-existing in the patients who would go on to respond. This hypothesis-generating observation implicates cluster 2 CD-14-monocyte as contributing to positive responses to ICB in melanoma patients.

Although exploratory, our data suggests that TIL/Bc contribute to ICB responses in melanoma patients. First, we identify a B cell signature (HLA with immunoglobulin expression) that characterises the immune-responsive tumours. Second, we show that amongst all TIMC, the memory B cells express the highest levels of class I and II HLA. Third, class I HLA antigen processing and presentation are the top differentially expressed pathways in the memory B cells of immune-responsive tumours. Fourth, the abundance of B cell clonotypes in pre-treatment biopsies, and thereby the potential of the B cell pool to recognise and present many different epitopes, is prognostic for survival after ICB. Our data are consistent with the observation that B cells are significantly enriched in tumours of responders versus non-responders to ICB. Note that while previous works focused largely on the presence and features of

tertiary lymphoid structures, we extend those studies by proposing a mechanistic role for B cells in neoantigen cross-presentation [21—24]. Additionally, we note previous findings that B cell clonotype abundance is prognostic in the melanoma TCGA, a cohort that was recorded before ICB approval [22,25,26], suggesting a therapy-agnostic role for B cells in anti-cancer immunity. Moreover, our data shows that in response to ICB, memory B cells become some of the most connected cells in the tumour, interacting with most other tumour cells. Taken together, these observations show that B cells are prognostic rather than predictive for patient response. We propose that this is because B cells do not have ICB-specific roles, but rather they contribute to a general tumour immune-permissive state by enhancing cancer neoantigen recognition by cytotoxic cells through antigen cross-presentation to cytotoxic T cells. In support of this, we show an increase in these biological functions in memory B cells in patients who will go on to respond to ICB.

Although we did not have adequate samples to achieve statistical power to infer prognostic value to the CD14-monocyte subsets and B cell signature we identified, we provide evidence in two independent cohorts that B cell clonotype abundance in pre-treatment biopsies is prognostic for ICB response. The association of ICB-induced responses with pre-treatment intra-tumour T cell clonal expansion [3], circulating CD14-monocytes with elevated IL1 signalling and tumour infiltration by many different B cell clonotypes suggests that these drugs require a level of pre-treatment immune activation to exert their effect. Thus, strategies to maximise patient outcomes might need to harness immune activation at different stages, including the pre-checkpoint blockade step, and our data identifies CD-14 monocytes and B cells as additional useful biomarkers for patient selection. Moreover, although our findings require prospective validation in larger cohorts, we propose mechanistic hypotheses for the role of B cells in the anti-cancer immune response activated by ICB and our results could lead to new immunotherapy approaches to enhance patient outcomes and contribute to the development of personalised therapeutic strategies through the identification of patients who could better benefit from these treatments.

Funding

Data and material availability

Biological material is not available for collaborations because patient-derived samples were entirely used for the experiments. Extended methods and source data can be obtained from the corresponding authors upon reasonable request, bulk RNA-Seq data can be obtained from EGA under the accession code EGAS00001005201, the RNA-Seq data for the validation cohort can be downloaded from the original publication [6].

Author contribution

Conflict of interest statement

The authors declare that they have no known competing financial interests or personal relationships that could have appeared to influence the work reported in this paper.

Acknowledgements

Appendix A. Supplementary data

Supplementary data to this article can be found online at https://doi.org/10.1016/j.ejca.2022.09.022.

References

[1] Kaushik I, Ramachandran S, Zabel C, Gaikwad S, Srivastava SK. The evolutionary legacy of immune checkpoint inhibitors. Semin Cancer Biol 2022;86(Pt 2):491—8. https://doi.org/10.1016/j.semcancer.2022.03.020.

[2] Sharpe AH, Pauken KE. The diverse functions of the PD1 inhibitory pathway. Nat Rev Immunol 2018;18(3):153—67.

[3] Valpione S, Mundra PA, Galvani E, Campana LG, Lorigan P, De Rosa F, et al. The T cell receptor repertoire of tumor infiltrating T cells is predictive and prognostic for cancer survival. Nat Commun 2021;12(1):4098.

[4] Davis A, Gao R, Navin NE. SCOPIT: sample size calculations for single-cell sequencing experiments. BMC Bioinf 2019;20(1):566.

[5] Schmid KT, Hollbacher B, Cruceanu C, Bottcher A, Lickert H, Binder EB, et al. scPower accelerates and optimizes the design of multi-sample single cell transcriptomic studies. Nat Commun 2021;12(1):6625.

[6] Liu D, Schilling B, Liu D, Sucker A, Livingstone E, Jerby-Arnon L, et al. Integrative molecular and clinical modeling of clinical outcomes to PD1 blockade in patients with metastatic melanoma. Nat Med 2019;25(12):1916−27.

[7] Zheng GX, Terry JM, Belgrader P, Ryvkin P, Bent ZW, Wilson R, et al. Massively parallel digital transcriptional profiling of single cells. Nat Commun 2017;8:14049.

[8] Stoeckius M, Hafemeister C, Stephenson W, Houck-Loomis B, Chattopadhyay PK, Swerdlow H, et al. Simultaneous epitope and transcriptome measurement in single cells. Nat Methods 2017; 14(9):865−8.

[9] Stoeckius M, Zheng S, Houck-Loomis B, Hao S, Yeung BZ, Mauck 3rd WM, et al. Cell Hashing with barcoded antibodies enables multiplexing and doublet detection for single cell genomics. Genome Biol 2018;19(1):224.

[10] Efremova M, Vento-Tormo M, Teichmann SA, Vento-Tormo R. CellPhoneDB: inferring cell-cell communication from combined expression of multi-subunit ligand-receptor complexes. Nat Protoc 2020;15(4):1484−506.

[11] Reimand J, Kull M, Peterson H, Hansen J, Vilo J g. Profiler–a web-based toolset for functional profiling of gene lists from large-scale experiments. Nucleic Acids Res 2007;35:W193−200. Web Server issue).

[12] Raudvere U, Kolberg L, Kuzmin I, Arak T, Adler P, Peterson H, et al. Profiler: a web server for functional enrichment analysis and conversions of gene lists (2019 update). Nucleic Acids Res 2019; 47(W1):W191−8.

[13] Choudhary S, Satija R. Comparison and evaluation of statistical error models for scRNA-seq. Genome Biol 2022;23(1):27.

[14] Korsunsky I, Millard N, Fan J, Slowikowski K, Zhang F, Wei K, et al. Fast, sensitive and accurate integration of single-cell data with Harmony. Nat Methods 2019;16(12):1289−96.

[15] Hao Y, Hao S, Andersen-Nissen E, Mauck 3rd WM, Zheng S, Butler A, et al. Integrated analysis of multimodal single-cell data. Cell 2021;184(13):3573−3587 e29.

[16] Rappl P, Brune B, Schmid T. Role of tristetraprolin in the resolution of inflammation. Biology 2021;10(1).

[17] Chen X, Jensen PE. The role of B lymphocytes as antigen-presenting cells. Arch Immunol Ther Exp 2008;56(2):77−83.

[18] Valpione S, Galvani E, Tweedy J, Mundra PA, Banyard A, Middlehurst P, et al. Immune-awakening revealed by peripheral T cell dynamics after one cycle of immunotherapy. Nat Cancer 2020;1(2):210−21.

[19] Mandric I, Rotman J, Yang HT, Strauli N, Montoya DJ, Van Der Wey W, et al. Profiling immunoglobulin repertoires across multiple human tissues using RNA sequencing. Nat Commun 2020;11(1):3126.

[20] Luke JJ, Ascierto PA, Carlino MS, Gershenwald JE, Grob JJ, Hauschild A, et al. KEYNOTE-716: phase III study of adjuvant pembrolizumab versus placebo in resected high-risk stage II melanoma. Future Oncol 2020;16(3):4429−38.

[21] Laumont CM, Banville AC, Gilardi M, Hollern DP, Nelson BH. Tumour-infiltrating B cells: immunological mechanisms, clinical impact and therapeutic opportunities. Nat Rev Cancer 2022.

[22] Helmink BA, Reddy SM, Gao J, Zhang S, Basar R, Thakur R, et al. B cells and tertiary lymphoid structures promote immunotherapy response. Nature 2020;577(7791):549−55.

[23] Cabrita R, Lauss M, Sanna A, Donia M, Skaarup Larsen M, Mitra S, et al. Tertiary lymphoid structures improve immunotherapy and survival in melanoma. Nature 2020;577(7791):561−5.

[24] Petitprez F, de Reynies A, Keung EZ, Chen TW, Sun CM, Calderaro J, et al. B cells are associated with survival and immunotherapy response in sarcoma. Nature 2020;577(7791):556−60.

[25] Bolotin DA, Poslavsky S, Davydov AN, Frenkel FE, Fanchi L, Zolotareva OI, et al. Antigen receptor repertoire profiling from RNA-seq data. Nat Biotechnol 2017;35(10):908−11.

[26] Griss J, Bauer W, Wagner C, Simon M, Chen M, Grabmeier-Pfistershammer K, et al. B cells sustain inflammation and predict response to immune checkpoint blockade in human melanoma. Nat Commun 2019;10(1):4186.